Closed-shell effect in two-neutrino double-β decay for fp shell nuclei

Hantao Li (李瀚涛),[1,*] Zhongzhou Ren (任中洲),[2,†] Chengwei Dong (董成伟),[1,‡] and Yue Hu (胡玥)[1]
[1]*School of Science, North University of China, Taiyuan 030051, China*
[2]*School of Physics Science and Engineering, Tongji University, Shanghai 200092, China*

(Received 22 December 2020; revised 2 August 2021; accepted 1 December 2021; published 13 December 2021)

Large scheme shell-model calculations are conducted for the two-neutrino double-β ($2\nu\beta\beta$) decay of the fp ($0f_{7/2}$, $0f_{5/2}$, $1p_{3/2}$, $1p_{1/2}$) shell nuclei. 25 $2\nu\beta\beta$ processes are considered, of which seven $2\nu\beta\beta$ processes are either observed or candidates. The calculated half-lives, nuclear matrix elements (NMEs), strength function (SF) distributions, and phase space factors are shown. The calculated results agree with the experimental data and reveal that for the transitions involving a doubly, semimagic nucleus or only the nonmagic nuclei, the SF distributions are visibly different. This outcome indicates that the NMEs of the $2\nu\beta\beta$ processes are significantly influenced by the closed-shell effect.

DOI: 10.1103/PhysRevC.104.064307

I. INTRODUCTION

The $2\nu\beta\beta$ decay process is a second-order weak-interaction process that has the most extended lifetime for all of the observed nuclear radioactive processes [1]. Approximately 90 nuclei are believed to undergo $2\nu\beta\beta$ decay, including decays for the β^- side ($2\nu2\beta^-$) and the mixed β^+ and electron capture types ($2\nu\beta^+$/EC, which includes $2\nu2\beta^+$, $2\nu\beta^+$EC, and 2νECEC), whereas the half-lives for only 14 of these nuclei have been observed with direct or geochemical measurements [2,3]. Although $2\nu\beta\beta$ decay is rare [4], this process is meaningful and it has attracted extensive research attention in previous studies [3–15]. The decay rate of the $2\nu\beta\beta$ decay can be written as a product of a phase space factor ($G_{2\nu}$) and a squared nuclear matrix element (NME) ($M_{2\nu}$), as expressed in Eq. (1) [16]:

$$\left[t_{1/2}^{2\nu}\right]^{-1} = G_{2\nu}|M_{2\nu}|^2, \tag{1}$$

where $G_{2\nu}$ is well known and depends on the decay energy to a great extent [17,18]. The NME is affected by the involved nuclear states, the study of which has led to a better understanding of the nuclear structure. Moreover, theorists predict the neutrinoless double-β ($0\nu\beta\beta$) decay. The mere discovery of $0\nu\beta\beta$ decay will undoubtedly confirm that a neutrino is a Majorana particle (a neutrino is its own antiparticle) and that the lepton number is not conserved in the weak process, therefore profoundly influencing the concept of fundamental physics [19]. In addition, the measurement of $0\nu\beta\beta$ decay is the most practical way to determine the mass of a neutrino provided that the associated nuclear matrix element ($M_{0\nu}$) is well understood. However, the accurate calculation of the $M_{0\nu}$ is not well settled at present. Different nuclear many-body predictions of the $M_{0\nu}$ differ from each other by a factor of two and such indeterminacy cannot be neglected. Furthermore, the famous g_A problem exists. This problem may be caused by the nuclear many-body correlations or the many-nucleon weak currents being missed, which will make the situation even worse [19]. With reliable experimental data, the $2\nu\beta\beta$ process is the process that is the closest to the $0\nu\beta\beta$ process and provides a valuable benchmark to calibrate the nuclear model calculations [4].

From the viewpoint of the nuclear shell-model, the $2\nu\beta\beta$ decay for the fp shell nuclei is of special interest. In this region, seven nuclei are believed to be $2\nu\beta\beta$ emitters and all of the decays involve a magic nucleus (Table I). It is well known that the magic number, which corresponds to the appearance of the closed-shell effect, is a crucial factor for the nuclear structure [20]. Since the NMEs of $2\nu\beta\beta$ decay depend on the structure of the implicated nuclei, it is plausible to suggest that the NME will be affected by the closed-shell effect.

Within the fp shell, the doubly magic nucleus ^{48}Ca has a large Q value (4.268 MeV), which results in a relatively short half-life and which has attracted extensive investigations with theoretical and experimental approaches [14,21–24]. The half-life for the $2\nu2\beta^-$ decay of the ^{48}Ca nucleus is well known, and numerous calculations about the $2\nu\beta\beta$ and $0\nu\beta\beta$ NMEs have been conducted [14,21,25,26]. Additionally, the abundances of the nuclei ^{58}Ni and ^{64}Zn are large (68.08% for ^{58}Ni and 49.17% for ^{64}Zn) [27], which is a significant advantage for experimental observation. Although the nuclei ^{58}Ni and ^{64}Zn decay to the $2\nu\beta^+$/EC direction, which is more difficult to measure, experiments have been conducted [28,29]. Recently, breakthroughs in $2\nu\beta^+$/EC experiments have been achieved, and the half-lives for the 2νECEC of the nuclei ^{82}Kr and ^{126}Xe have been determined [3,30]. Thus, 2νECEC of the nuclei ^{58}Ni and ^{64}Zn may be measured in the near future. The $2\nu\beta\beta$ decay of the nucleus ^{70}Zn is also of interest. Within the fp shell, the nucleus is defined as a semimagic nucleus. However, in the fpg ($0f_{5/2}$, $1p_{3/2}$, $1p_{1/2}$, $0g_{9/2}$) shell,

*lihantao@nuc.edu.cn
†zren@tongji.edu.cn; zren@nju.edu.cn
‡dongchengwei@tsinghua.org.cn

TABLE I. The $2\nu\beta\beta$ emitters in the fp shell whose transitions involve a doubly magic nucleus and six semimagic nuclei. It should be noted that in the fp shell, ^{70}Zn with $N = 40$ is by default a semimagic nucleus.

Property	$2\nu\beta\beta$	Magic number involved
Doubly magic	$^{48}_{20}\mathrm{Ca}_{28} \rightarrow {}^{48}_{22}\mathrm{Ti}_{26}$	$Z = 20, N = 28$
Semimagic	$^{46}_{20}\mathrm{Ca}_{26} \rightarrow {}^{46}_{22}\mathrm{Ti}_{24}$	$Z = 20$
	$^{50}_{24}\mathrm{Cr}_{26} \rightarrow {}^{50}_{22}\mathrm{Ti}_{28}$	$N = 28$
	$^{54}_{26}\mathrm{Fe}_{28} \rightarrow {}^{54}_{24}\mathrm{Cr}_{30}$	
	$^{58}_{28}\mathrm{Ni}_{30} \rightarrow {}^{58}_{26}\mathrm{Fe}_{32}$	$Z = 28$
	$^{64}_{30}\mathrm{Zn}_{34} \rightarrow {}^{64}_{28}\mathrm{Ni}_{36}$	
	$^{70}_{30}\mathrm{Zn}_{40} \rightarrow {}^{70}_{32}\mathrm{Ge}_{38}$	$N = 40$

the nucleus is treated as a nonmagic nucleus. It would be especially meaningful to compare the results of ^{70}Zn for these two different model spaces.

In this research, shell-model calculations are conducted for the $2\nu\beta\beta$ decay for nuclei within the fp shell. Decays for both the $2\nu2\beta^-$ and mixed $2\nu\beta^+$/EC types are considered. Three distinct effective interactions are employed to ensure the reliability of the calculations. The theoretical half-lives, phase space factors, and NMEs are shown and discussed in detail. By analyzing the SF distributions, it is concluded that the closed-shell effect significantly influences the NME of $2\nu\beta\beta$ decay.

II. OUTLINE OF THE THEORETICAL FRAMEWORK

A. Formulas for the $2\nu\beta\beta$ decay

It is well known that the half-life of the $2\nu\beta\beta$ decay is determined by the phase space factor $G_{2\nu}$ and the NME $M_{2\nu}$, as expressed in Eq. (1). In this research, both of the $2\nu2\beta^-$ and the $2\nu\beta^+$/EC ($2\nu2\beta^+$, $2\nu\beta^+$EC, and 2νECEC) types are considered. The evaluation of the $G_{2\nu}$ is simple. The formulas in Ref. [16] are used to calculate the $G_{2\nu}$ of $2\nu2\beta^-$ and the formulas in Refs. [16,31,32] are used for the $2\nu\beta^+$/EC. The axial-vector coupling constant g_A, for which the $G_{2\nu}$ is proportional to its fourth power, is important in the calculation. The widely used value $g_A = 1.27$ [26,33] is adopted in the calculations.

The situation for the $M_{2\nu}$ is much more complicated in that it depends on the decay mode and the angular momentum of the final state [31]. In this research, since only the ground state is considered, the $M_{2\nu}$ can be simplified as

$$M^{\alpha}_{2\nu} = \sum_m M_m F^{\alpha}_m. \tag{2}$$

The summation is for all the intermediate 1^+ states and the superscript α denotes the specific type of decay. In the framework of the nuclear shell-model, the quantity M_m (for the transition to the ground state) has the form of [16,31,34]

$$M_m = \langle 0^+_f \| \sum_a \sigma_a \tau^{\pm}_a \| 1^+_m \rangle \langle 1^+_m \| \sum_b \sigma_b \tau^{\pm}_b \| 0^+_i \rangle \tag{3}$$

with τ^- (τ^+) as the isospin lowering (raising) operator corresponding to $2\nu2\beta^-$ ($2\nu\beta^+$/EC), the summation will go through all possible nucleons. The quantities F^{α}_m in Eq. (2) are the energy denominators that depend on the type of the $2\nu\beta\beta$. For the transitions to the ground state, F^{α}_m can be cast in the form of [31,35]

$$F^{2\beta^-}_m = F^{2\beta^+}_m = \left(\Delta_m + \tfrac{1}{2}W_0\right)^{-1}, \tag{4}$$

$$F^{\beta^+\mathrm{EC}}_m = \left(\Delta_m - \varepsilon_{b1} + \tfrac{1}{3}W^{\beta^+\mathrm{EC}}_0\right)^{-1} + \left(\Delta_m + \tfrac{2}{3}W^{\beta^+\mathrm{EC}}_0\right)^{-1}, \tag{5}$$

$$F^{\mathrm{ECEC}}_m = \left(\Delta_m - \varepsilon_{b1} + \tfrac{1}{2}W^{\mathrm{ECEC}}_0\right)^{-1} + \left(\Delta_m - \varepsilon_{b2} + \tfrac{1}{2}W^{\mathrm{ECEC}}_0\right)^{-1}, \tag{6}$$

where

$$\begin{aligned} \Delta_m &= (E_m - M_i c^2)/(m_e c^2), \\ W_0 &= (M_i c^2 - E_f)/(m_e c^2), \\ W^{\beta^+\mathrm{EC}}_0 &= W_0 + \varepsilon_{b1}, \\ W^{\mathrm{ECEC}}_0 &= W_0 + \varepsilon_{b1} + \varepsilon_{b2}. \end{aligned} \tag{7}$$

In Eq. (7), E_m and E_f are the energies of the intermediate and daughter nuclear states, respectively. The symbol M_i is the mass of the parent nucleus and m_e represents the electron masses. The expression $\varepsilon_b = (m_e c^2 - B_i)/m_e c^2$ represents the total energy for the captured electron, where B_i is the binding energy of the absorbed electron [31,32].

B. Discussion of the shell-model calculations

To include more nuclear many-body correlations, in shell-model calculations, a large model space is preferred if the computation ability is sufficient. Thus, all the calculations are conducted in the whole fp shell-model space to ensure the quality of the results. Additionally, effective interaction is of great importance in shell-model calculations. Three widely used interactions GX1A [36,37], KB3G [38], and FPD6 [39] are used to calculate the wave functions of the nuclei being studied.

Based on Eqs. (2) and (3), the calculation of the NME involves all the intermediate 1^+ states. However, some of the model spaces are huge and it is not practical to include all the possible 1^+ states. We consider 100 intermediate 1^+ states in the calculations of the NME. The convergence of the NME is of great importance and it should be carefully discussed. Thus, the accumulations of the normalized NME are plotted in Fig. 1. It is obvious that when the number of accumulated 1^+ states exceeds 70, the fluctuations in all the curves are very small, which indicates the convergence of the NME. We also notice that the nuclear structure community has explored much larger model spaces for the $2\nu\beta\beta$ decay of ^{48}Ca. Kostensal and Suhonen calculate the $2\nu\beta\beta$ decay of the ^{48}Ca in fp shell using the GX1A effective interaction [6], for which all the 9470 intermediate states are considered and a quenching factor $q = 0.77$ is employed. The NME yields 0.0511 MeV^{-1}. Based on the same parameters, the results for 100 intermediate states produce 0.0530 MeV^{-1}, which differs

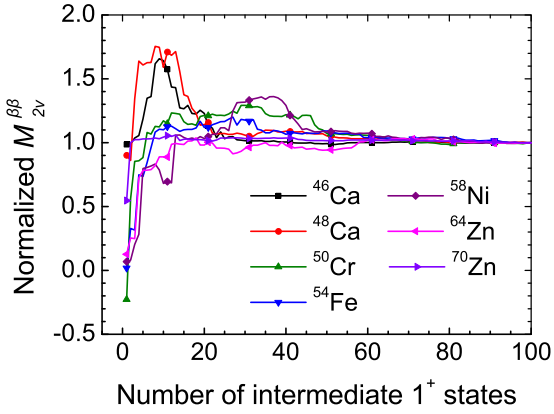

FIG. 1. Accumulation of the normalized NMEs.

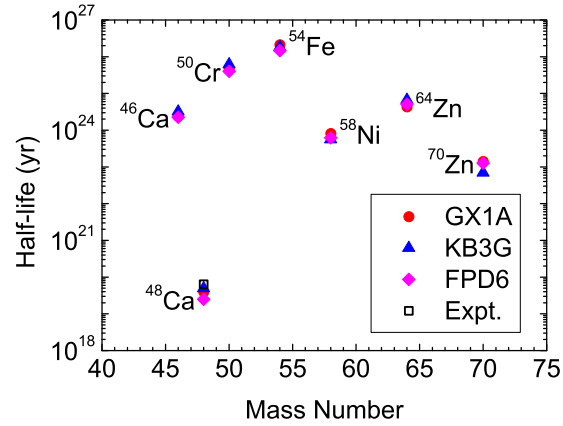

FIG. 2. Half-lives of the $2\nu\beta\beta$ emitters being studied in the $\log_{10}$ frame. The red circles, blue triangles, and pink diamonds represent the calculated results based on the GX1A, KB3G, and FPD6 effective interactions, respectively. The hollow black squares represent the experimental results.

from Ref. [6] by only approximately 4%. Thus, the NME is considered to be well converged.

According to Eq. (7), the energy of the intermediate state plays a vital role in the calculation of the NME. In this work, this value is shifted due to the experimental value of the lowest 1^+ state [40]. Additionally, the famous g_A problem is encountered in the shell-model calculations [19], which refers to the systemic over-prediction of the single-β and $2\nu\beta\beta$ matrix elements. Usually, a quenching factor is used as a correction factor of the nucleon many-body interactions. The widely used value $q = 0.744$ [41] is adopted in this work.

III. RESULTS AND DISCUSSION

Within the fp shell, seven nuclei are regarded as $2\nu\beta\beta$ emitters. Among them, only the half-life of the nucleus ^{48}Ca is measured. With the most extended half-life for all the nuclear radioactive processes ever observed, the half-life is one of the most exciting features for $2\nu\beta\beta$ decay. In this work, three different effective interactions are induced to calculate the half-life for all of the emitters. Table II compares the theoretical results for the half-lives with the experimental data. The Q values adopted in the calculations and the averaged energies for the top intermediate 1^+ state $\overline{E}(1^+_{100})$ are listed. As a clear illustration, the half-lives of the $2\nu\beta\beta$ are also presented in Fig. 2, for which all the data are derived from Table II.

These results from different effective interactions are consistent with each other and they agree with the experimental data. The half-lives of the nuclei ^{58}Ni and ^{70}Zn are predicted to be 8.06×10^{23} and 1.41×10^{23} years, respectively (using GX1A), which are relatively short and may be observed in the near future. This is especially true for ^{58}Ni, whose abundance is quite large (60.08%). As clearly shown in Eq. (1), the half-life of the $2\nu\beta\beta$ decay is determined by the NME and the phase space factor $G_{2\nu}$. The calculation of the NME is essential for the theoretical research of the $2\nu\beta\beta$ decay. For the $2\nu\beta^+$/EC decay, the formulas for the $G_{2\nu}$ and the NME of $2\beta^+$, β^+EC, and ECEC are different. As a clear illustration, the value of the NMEs (in the natural unit with the electron mass equal to 1) and the $G_{2\nu}$ for different nuclei are listed in Table III in detail.

As can be seen from Table III, the results based on different effective interactions are consistent. The NMEs for $2\nu\beta^+$EC and 2νECEC are very close. Owing to the energy denominator [Eqs. (4)–(7)], the NMEs are approximately two times the scale of the NME for $2\nu 2\beta^+$. For most cases, the half-life of the $2\nu\beta^+$/EC decay is determined by the 2νECEC. Thus, the NMEs for $2\nu 2\beta^-$ and 2νECEC are plotted, as shown in Fig. 3.

TABLE II. The half-lives of the $2\nu\beta\beta$ emitters in the fp shell, along with the averaged energies of the top intermediate 1^+ state $\overline{E}(1^+_{100})$ and the Q values adopted in the calculations.

Nucleus	Type	Q value (keV)	Half-life (yr) GX1A	KB3G	FPD6	Expt.	$\overline{E}(1^+_{100})$ (MeV)
^{46}Ca	$2\beta^-$	988.4	2.41×10^{24}	3.20×10^{24}	2.27×10^{24}		10.82
^{48}Ca	$2\beta^-$	4268.08	3.99×10^{19}	4.97×10^{19}	2.49×10^{19}	$6.4^{+0.7}_{-0.6}(stat)^{+1.2}_{-0.9}(syst) \times 10^{19}$ [21] $5.6 \pm 1.0 \times 10^{19}$ [27]	11.08
^{50}Cr	$2\beta^+$	1169.6	4.73×10^{25}	6.21×10^{25}	4.00×10^{25}	$>1.3 \times 10^{18}$	8.65
^{54}Fe	$2\beta^+$	680.3	2.10×10^{26}	1.83×10^{26}	1.46×10^{26}	$>4.4 \times 10^{20}$	7.71
^{58}Ni	$2\beta^+$	1926.4	8.09×10^{23}	5.59×10^{23}	6.18×10^{23}	$>2.1 \times 10^{21}$	6.45
^{64}Zn	$2\beta^+$	1094.9	4.27×10^{24}	6.69×10^{24}	5.13×10^{24}	$>7.0 \times 10^{20}$	6.44
^{70}Zn	$2\beta^-$	997.1	14.1×10^{22}	6.94×10^{22}	12.7×10^{22}		10.76

TABLE III. Phase space factors $G_{2\nu}$ and NMEs of $2\nu\beta\beta$ decay for the nuclei being studied.

Nucleus	Process	$G_{2\nu}(yr^{-1})$	$\lvert M^{2\nu}_{GT}\rvert$ GX1A	KB3G	FPD6
^{46}Ca	$2\beta^-$	1.24×10^{-22}	0.0578	0.0501	0.0595
^{48}Ca	$2\beta^-$	4.17×10^{-17}	0.0245	0.0220	0.0310
^{50}Cr	$2\beta^+$	–	0.0651	0.0569	0.0709
	β^+EC	3.34×10^{-30}	0.132	0.115	0.143
	ECEC	1.25×10^{-24}	0.130	0.114	0.142
^{54}Fe	$2\beta^+$	–	0.0937	0.100	0.113
	β^+EC	–	0.189	0.203	0.227
	ECEC	1.36×10^{-25}	0.187	0.201	0.225
^{58}Ni	$2\beta^+$	–	0.0814	0.0978	0.0931
	β^+EC	3.04×10^{-24}	0.166	0.202	0.191
	ECEC	4.35×10^{-23}	0.163	0.196	0.186
^{64}Zn	$2\beta^+$	–	0.121	0.0966	0.110
	β^+EC	1.04×10^{-32}	0.250	0.200	0.230
	ECEC	4.01×10^{-24}	0.242	0.193	0.221
^{70}Zn	$2\beta^-$	3.24×10^{-22}	0.148	0.211	0.162

According to Eq. (2), the NMEs are determined by the structures of the parent, medium, and daughter nuclei. However, the formulas for $2\nu2\beta^-$ and 2νECEC are significantly different and a direct comparison is not helpful for gaining insights into the nuclear structure. To probe the relationship between the closed-shell effect and the NME, we present the NMEs for $2\nu2\beta^-$ and $2\nu2\beta^+$ in Fig. 4. The decay of ^{48}Ca involves a doubly magic nucleus and the rest of the decays only involve a semimagic nucleus. It is clear that if the decay process involves a doubly magic nucleus, the corresponding NME will have a smaller value than others.

To explore the reason for this outcome and to make the results more convincing, we also calculate some hypothetical transitions in the fp shell. The NME can be seen in Fig. 5, where the red squares, blue triangles, and pink stars represent the transition involving a doubly, semi- magic nucleus, and only the nonmagic nuclei, respectively. Nevertheless, for decay involving a doubly magic nucleus, the NMEs become visibly smaller.

As a further exploration, we also examine the SF distributions for the NMEs. Figure 6 shows the normalized SF as a function of the energy of intermediate states. The SF distributions can be classified into three categories:

I. The strengths are highly fragmented and strongly cancel each other out; see Fig. 6(a).

II. The strengths are concentrated into very few states that are close to the single-state dominates (SSD) [4]; see Fig. 6(b).

III. The strengths are highly fragmented but they rarely cancel each other out; see Fig. 6(c).

According to the above classifications, two quantities are employed to describe the SF distributions. The standard deviation (SD) of the normalized SF is

$$\mathrm{SD}=\sqrt{\frac{\sum_i(\mathrm{SF}_i-\overline{\mathrm{SF}})^2}{n-1}}/\overline{\mathrm{SF}}. \tag{8}$$

The "difference" between the SD and the standard deviation for the absolute value of the normalized SF can then be

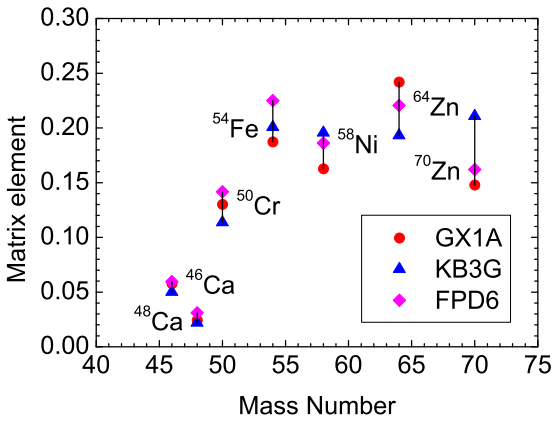

FIG. 3. The NMEs of $2\nu2\beta^-$ and 2νECEC for different nuclei, where the red circles, blue triangles, and pink diamonds represent the calculated results for the GX1A, KB3G, and FPD6 effective interactions, respectively.

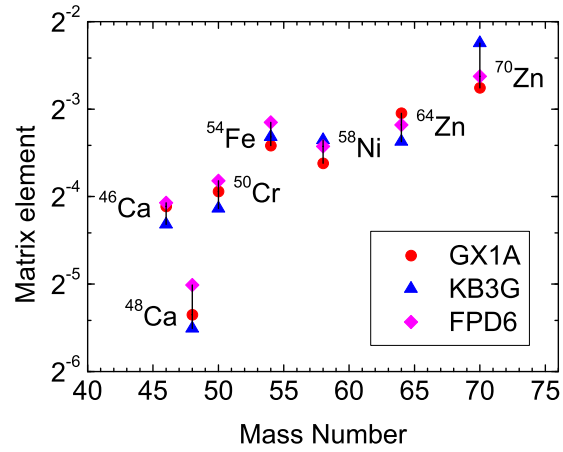

FIG. 4. The NMEs for the $2\nu2\beta^+$ and $2\nu2\beta^-$ decays in the $\log_2$ frame. The decay of ^{48}Ca involves a doubly magic nucleus and the rest of the decays involve semi-magic nuclei only.

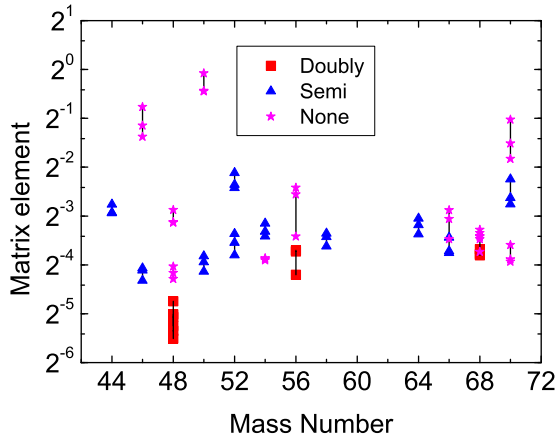

FIG. 5. The NMEs for $2\nu 2\beta^{+}$ and $2\nu 2\beta^{-}$ decays of the fp shell nuclei.

written as

$$\text{difference} = \text{SD} - \sqrt{\frac{\sum(|\text{SF}_i| - \overline{|\text{SF}|})^2}{n-1}}/\overline{|\text{SF}|}. \qquad (9)$$

For case I, both the SD and the "difference" are considerable. For case II, the SD is significant, but the "difference" is small. For case III, both the SD and the "difference" are relatively small. Taking the ideal SSD (belonging to case II) as an example, for 100 intermediate states ($n = 100$), the SD will be 10, and the "difference" should be zero. We present the SD and the "difference" for all the nuclei being studied in Table IV and we depict them in Fig. 7. It is evident that for transitions involving a doubly magic nucleus, both the SD and the "difference" are significant, which means that the transitions belong to the category of case I and suggests the solid canceling nature of the SF distribution of the transitions. Since the Ikeda sum rule limits the total Gamow-Teller strength, this cancellation leads to a depression of the NME. It should be noted that the SF distribution for the doubly closed-shell nucleus $^{68}_{28}\text{Ni}_{40}$ is quite different from that of the others. However, extensive studies have shown the semimagic nature [42,43] of ^{68}Ni. The calculated results in this research also support this concept.

For the case where the transitions involve a semimagic nucleus, the SD is relatively large and the "difference" is widespread. Therefore, the SF distribution belongs to cases I or II. The only exception is the $2\nu\beta\beta$ decay of ^{64}Zn, whose daughter nucleus $^{64}_{28}$Ni is reported to have shape coexistence at zero spins. This shape coexistence is interpreted to originate from the monopole tensor force [44] that shifts effective single-particle energies and weakens resistance against deformation. The low-lying intruder states in ^{64}Ni are referred to as Type II shell evolution (the shell evolution inside the same nucleus) [45]. Thus, the nucleus ^{64}Ni is considered to be exceptional and the calculated result shows its non-magic feature, which is worthwhile for further investigations.

The situations for the nonmagic nuclei are the most complicated and we further divide these situations into two categories. For the nuclei whose proton or neutron numbers are between 20 and 28 (Non-1 in Fig. 7 and Table IV), the SF distributions are very similar to the cases of the semimagic nucleus. The reason for this is that from the viewpoint of the naive shell model, the valence protons/neutrons for these nuclei are distributed only in the $0f_{7/2}$ orbit. This orbit itself forms a closed-shell, and it is difficult for these valence protons/neutrons to exit to other orbits. Thus, these nuclei in particular have properties similar to the semimagic nuclei. For the rest of the nonmagic nuclei (non-2 in Fig. 7 and Table IV), both the SD and the "difference" are small, so the nuclei belong to the category of case III.

The $2\nu\beta\beta$ decay of ^{70}Zn is of particular interest. One can calculate this transition in either the fp or fpg $(0f_{5/2}, 1p, 0g_{9/2})$ shell-model space. In the fp shell, ^{70}Zn is defined as a semimagic nucleus, while in the fpg shell it is nonmagic. We also calculate the $2\nu\beta\beta$ decay of ^{70}Zn and ^{64}Zn in the fpg shell-model space using the JUN45 effective interaction [46]. The results are presented in Fig. 7 and Table IV as well (in the fpg part). The calculated NMEs from the fp and fpg shells for ^{70}Zn are almost the same [35]. However, the SF

TABLE IV. The values of the SD and the "difference" [defined by Eqs. (8) and (9)] for the $2\nu\beta\beta$ decay of the nuclei being studied.

Type	Transition	SD	Difference
Doubly	$^{48}_{20}\text{Ca}_{28} \to {}^{48}_{22}\text{Ti}_{26}$	10.85	7.25
	$^{48}_{28}\text{Ni}_{20} \to {}^{48}_{26}\text{Fe}_{22}$	10.51	6.80
	$^{56}_{28}\text{Ni}_{28} \to {}^{56}_{26}\text{Fe}_{30}$	10.23	6.86
	$^{68}_{28}\text{Ni}_{40} \to {}^{68}_{30}\text{Zn}_{38}$	9.52	2.10
Semi	$^{44}_{22}\text{Ti}_{22} \to {}^{44}_{20}\text{Ca}_{24}$	9.15	3.97
	$^{46}_{20}\text{Ca}_{26} \to {}^{46}_{22}\text{Ti}_{24}$	8.96	5.42
	$^{50}_{24}\text{Cr}_{26} \to {}^{50}_{22}\text{Ti}_{28}$	7.76	4.56
	$^{52}_{22}\text{Ti}_{30} \to {}^{52}_{24}\text{Cr}_{28}$	7.64	1.73
	$^{52}_{26}\text{Fe}_{26} \to {}^{52}_{24}\text{Cr}_{28}$	6.74	4.06
	$^{54}_{26}\text{Fe}_{28} \to {}^{54}_{24}\text{Cr}_{30}$	6.81	3.31
	$^{58}_{28}\text{Ni}_{30} \to {}^{58}_{26}\text{Fe}_{32}$	7.25	4.00
	$^{64}_{30}\text{Zn}_{34} \to {}^{64}_{28}\text{Ni}_{36}$	4.28	1.27
	$^{66}_{28}\text{Ni}_{38} \to {}^{66}_{30}\text{Zn}_{36}$	6.10	2.33
	$^{70}_{30}\text{Zn}_{40} \to {}^{70}_{32}\text{Ge}_{38}$	8.34	1.31
Non-1	$^{46}_{24}\text{Cr}_{22} \to {}^{46}_{22}\text{Ti}_{24}$	7.07	1.97
	$^{48}_{24}\text{Cr}_{24} \to {}^{48}_{22}\text{Ti}_{26}$	6.48	3.11
	$^{48}_{26}\text{Fe}_{22} \to {}^{48}_{24}\text{Cr}_{24}$	6.95	4.21
	$^{50}_{26}\text{Fe}_{24} \to {}^{50}_{24}\text{Cr}_{26}$	8.01	1.38
	$^{54}_{22}\text{Ti}_{32} \to {}^{54}_{24}\text{Cr}_{30}$	6.74	2.26
	$^{56}_{22}\text{Ti}_{34} \to {}^{56}_{24}\text{Cr}_{32}$	8.05	1.08
Non-2	$^{66}_{32}\text{Ge}_{34} \to {}^{66}_{30}\text{Zn}_{36}$	4.21	0.94
	$^{68}_{32}\text{Ge}_{36} \to {}^{68}_{30}\text{Zn}_{38}$	3.85	1.21
	$^{68}_{34}\text{Se}_{34} \to {}^{68}_{32}\text{Ge}_{36}$	3.49	1.15
	$^{70}_{34}\text{Se}_{36} \to {}^{70}_{32}\text{Ge}_{38}$	4.23	1.29
	$^{70}_{36}\text{Kr}_{34} \to {}^{70}_{34}\text{Se}_{36}$	4.03	0.47
fpg	$^{64}_{30}\text{Zn}_{34} \to {}^{64}_{28}\text{Ni}_{36}$	4.40	0.82
	$^{70}_{30}\text{Zn}_{40} \to {}^{70}_{32}\text{Ge}_{38}$	4.56	0.24

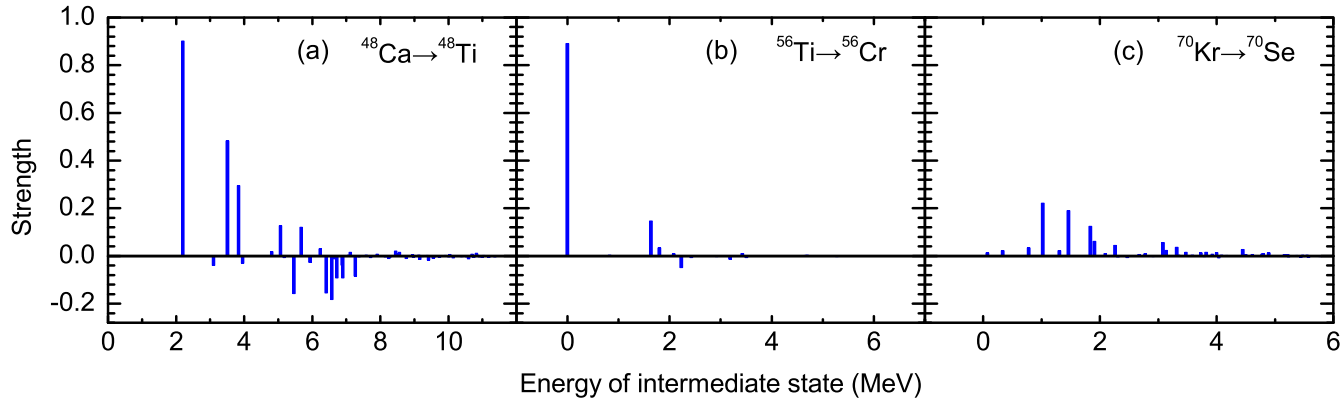

FIG. 6. The normalized strength distribution as a function of the energy of the intermediate states.

distributions are not consistent with each other. The calculated results from the fp shell show no difference between ^{70}Zn and the other semimagic nuclei, while calculations from the fpg shell present the nonmagic character of ^{70}Zn. Reference [47] shows that the inclusion of the $0g_{9/2}$ orbit to account for the nonmagic nature of ^{70}Zn explains this discrepancy. Indeed, the results from the fpg shell are much more reliable. The $2\nu\beta\beta$ decay of ^{64}Zn can also be calculated within the fp or fpg shell-model space. The theoretical SF distributions from these two spaces are consistent with each other and suggest the nonmagic nature of the ^{64}Ni.

Thus, it can be concluded that for transitions involving a doubly, semimagic nucleus or only the nonmagic nuclei, the SF distributions are significantly different. This result strongly supports the assumption that the closed-shell effect has a significant impact on the $2\nu\beta\beta$ decay. In contrast, $2\nu\beta\beta$ decay can be a powerful tool for exploring shell evolution and some other nuclear shell effects.

IV. SUMMARY AND CONCLUSION

We calculate the $2\nu\beta\beta$ decay for the fp shell nuclei in the entire $0\hbar\omega$ shell-model space with three distinct effective interactions, and we discuss the influence of the closed-shell effect. It is found that the SF distributions are distinct for the transition involving a doubly, semimagic nucleus or only the nonmagic nuclei. For cases involving a doubly magic nucleus, the strengths are highly fragmented and largely cancel each other out, leading to a depression of the NME. For a transition involving a semimagic nucleus, the strengths either destroy each other or are concentrated to a few states. For a transition involving only nonmagic nuclei with valance protons/neutrons only in the $f_{7/2}$ orbit, the SF distributions are very close to the semimagic case, which is due to the large shell gap of N or $Z = 28$. The strength distributions for the rest of the nonmagic nuclei are highly fragmented, but the cancellation is minimal. This result suggests that the closed-shell effect has a significant influence on the $2\nu\beta\beta$ decay. The calculated results present the semimagic nature of $^{68}_{28}$Ni$_{40}$ which is consistent with other works. In previous studies, $^{64}_{28}$Ni$_{36}$ has been reported to have an unexpectedly complex landscape of coexisting shapes. Our results show that this nucleus has the feature of being nonmagic, which is worthy of further investigation. We believe that research about the $2\nu\beta\beta$ process can also be an effective way to explore the shell evolution.

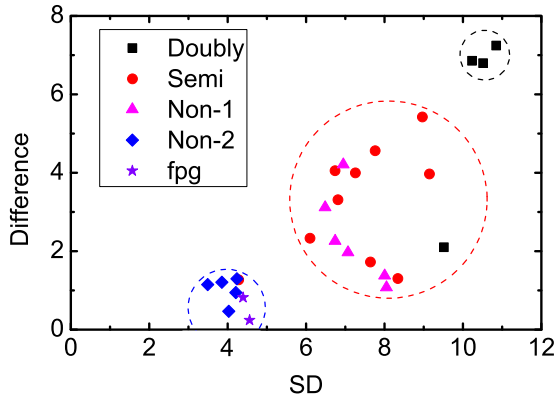

FIG. 7. The relationship between the SD and the "difference" for the $2\nu\beta\beta$ decay of the nuclei being studied. The situations are distinct for the transition involving a doubly, semimagic nucleus, or only the nonmagic nuclei.

ACKNOWLEDGMENTS

The authors are very grateful to Prof. B. A. Brown, Michigan State University, for providing us with the computer program NuShellX. The authors also express their sincere thanks to Dr. Q. Jie, North University of China, for some valuable discussions. This work is supported by the National Natural Science Foundation of China (Grants No. 11647086, No. 11647085, No. 11975167, No. 12035011, and No. 11761161001), by the National Major State Basic Research and Development of China (Grant No. 2016YFE0129300), by the Shanxi Province Science Foundation for Youths (Grant No. 201901D211252), by the Natural Science Foundation of Shanxi Province, China (Grants No. 201601D021020 and No. 201901D111180), and by the Scientific and Technological Innovation Programs of Higher Education Institutions in Shanxi (Grants No. 2019L0554 and No. 2019L0505).

[1] R. Saakyan, Annu. Rev. Nucl. Part. Sci. **63**, 503 (2013).

[2] C. Patrignani, K. Agashe, G. Aielli, C. Amsler, M. Antonelli, D. M. Asner, H. Baer, Sw. Banerjee, R. M. Barnett, T. Basaglia, C. W. Bauer, J. J. Beatty, V. I. Belousov, J. Beringer, S. Bethke, H. Bichsel, O. Biebel, E. Blucher, G. Brooijmans, O. Buchmueller *et al.* (Particle Data Group), Chin. Phys. C **40**, 100001 (2016).

[3] E. Aprile, J. Aalbers, F. Agostini, M. Alfonsi, L. Althueser, F. D. Amaro, M. Anthony, V. C. Antochi, F. Arneodo, L. Baudis, B. Bauermeister, M. L. Benabderrahmane, T. Berger, P. A. Breur, A. Brown, A. Brown, E. Brown, S. Bruenner, G. Bruno, R. Budnik *et al.* (XENON Collaboration), Nature (London) **568**, 532 (2019).

[4] O. Azzolini, J. W. Beeman, F. Bellini, M. Beretta, M. Biassoni, C. Brofferio, C. Bucci, S. Capelli, L. Cardani, P. Carniti, N. Casali, D. Chiesa, M. Clemenza, O. Cremonesi, A. Cruciani, I. Dafinei, S. DiDomizio, F. Ferroni, L. Gironi, A. Giuliani *et al.*, Phys. Rev. Lett. **123**, 262501 (2019).

[5] F. Šimkovic, R. Dvornický, D. Štefánik, and A. Faessler, Phys. Rev. C **97**, 034315 (2018).

[6] J. Kostensalo and J. Suhonen, Phys. Lett. B **802**, 135192 (2020).

[7] H. Ejiri, J. Phys. G: Nucl. Part. Phys. **46**, 125202 (2019).

[8] A. Gando, Y. Gando, T. Hachiya, M. Ha Minh, S. Hayashida, Y. Honda, K. Hosokawa, H. Ikeda, K. Inoue, K. Ishidoshiro, Y. Kamei, K. Kamizawa, T. Kinoshita, M. Koga, S. Matsuda, T. Mitsui, K. Nakamura, A. Ono, N. Ota, S. Otsuka *et al.* (KamLAND-Zen Collaboration), Phys. Rev. Lett. **122**, 192501 (2019).

[9] M. Agostini, M. Allardt, A. M. Bakalyarov, M. Balata, I. Barabanov, N. Barros, L. Baudis, C. Bauer, N. Becerici-Schmidt, E. Bellotti, S. Belogurov, S. T. Belyaev, G. Benato, A. Bettini, L. Bezrukov, T. Bode, D. Borowicz, V. Brudanin, R. Brugnera, D. Budjá *et al.* (GERDA Collaboration), J. Phys. G: Nucl. Part. Phys. **42**, 115201 (2015).

[10] N. Ackerman, B. Aharmim, M. Auger, D. J. Auty, P. S. Barbeau, K. Barry, L. Bartoszek, E. Beauchamp, V. Belov, C. Benitez-Medina, M. Breidenbach, A. Burenkov, B. Cleveland, R. Conley, E. Conti, J. Cook, S. Cook, A. Coppens, I. Counts, W. Craddock *et al.* (EXO Collaboration), Phys. Rev. Lett. **107**, 212501 (2011).

[11] J. Argyriades, R. Arnold, C. Augier, J. Baker, A. S. Barabash, A. Basharina-Freshville, M. Bongrand, G. Broudin, V. Brudanin, A. J. Caffrey, E. Chauveau, Z. Daraktchieva, D. Durand, V. Egorov, N. Fatemi-Ghomi, R. Flack, Ph. Hubert, J. Jerie, S. Jullian, M. Kauer *et al.* (NEMO Collaboration), Phys. Rev. C **80**, 032501(R) (2009).

[12] M. Horoi and B. A. Brown, Phys. Rev. Lett. **110**, 222502 (2013).

[13] E. Caurier, F. Nowacki, A. Poves, and J. Retamosa, Phys. Rev. Lett. **77**, 1954 (1996).

[14] K. Yako, M. Sasano, K. Miki, H. Sakai, M. Dozono, D. Frekers, M. B. Greenfield, K. Hatanaka, E. Ihara, M. Kato, T. Kawabata, H. Kuboki, Y. Maeda, H. Matsubara, K. Muto, S. Noji, H. Okamura, T. H. Okabe, S. Sakaguchi, Y. Sakemi *et al.*, Phys. Rev. Lett. **103**, 012503 (2009).

[15] Y. Hu, H. Li, and C. Dong, Chin. Phys. C **44**, 124108 (2020).

[16] J. Suhonen and O. Civitarese, Phys. Rep. **300**, 123 (1998).

[17] J. Kotila and F. Iachello, Phys. Rev. C **85**, 034316 (2012).

[18] J. Kotila and F. Iachello, Phys. Rev. C **87**, 024313 (2013).

[19] J. Engel and J. Menéndez, Rep. Prog. Phys. **80**, 046301 (2017).

[20] Y. J. Ren and Z. Z. Ren, Phys. Rev. C **89**, 064603 (2014).

[21] R. Arnold, C. Augier, A. M. Bakalyarov, J. D. Baker, A. S. Barabash, A. Basharina-Freshville, S. Blondel, S. Blot, M. Bongrand, V. Brudanin, J. Busto, A. J. Caffrey, S. Calvez, M. Cascella, C. Cerna, J. P. Cesar, A. Chapon, E. Chauveau, A. Chopra, D. Duchesneau *et al.* (NEMO-3 Collaboration), Phys. Rev. D **93**, 112008 (2016).

[22] A. Balysh, A. De Silva, V. I. Lebedev, K. Lou, M. K. Moe, M. A. Nelson, A. Piepke, A. Pronskiy, M. A. Vient, and P. Vogel, Phys. Rev. Lett. **77**, 5186 (1996).

[23] J. M. Yao, B. Bally, J. Engel, R. Wirth, T. R. Rodríguez, and H. Hergert, Phys. Rev. Lett. **124**, 232501 (2020).

[24] D. Zinatulina, V. Brudanin, V. Egorov, C. Petitjean, M. Shirchenko, J. Suhonen, and I. Yutlandov, Phys. Rev. C **99**, 024327 (2019).

[25] B. A. Brown, M. Horoi, and R. A. Sen'kov, Phys. Rev. Lett. **113**, 262501 (2014).

[26] Y. Iwata, N. Shimizu, T. Otsuka, Y. Utsuno, J. Menéndez, M. Honma, and T. Abe, Phys. Rev. Lett. **116**, 112502 (2016).

[27] F. G. Kondev, M. Wang, W. J. Huang, S. Naimi, and G. Audi, Chin. Phys. C **45**, 030001 (2021).

[28] B. Lehnert, D. Degering, A. Frotscher, T. Michel, and K. Zuber, J. Phys. G: Nucl. Part. Phys. **43**, 065201 (2016).

[29] P. Belli, R. Bernabei, F. Cappella, R. Cerulli, F. A. Danevich, B. V. Grinyov, A. Incicchitti, V. V. Kobychev, V. M. Mokina, S. S. Nagorny, L. L. Nagornaya, S. Nisi, F. Nozzoli, D. V. Poda, D. Prosperi, V. I. Tretyak, and S. S. Yurchenko, Nucl. Phys. A **826**, 256 (2009).

[30] Yu. M. Gavrilyuk, A. M. Gangapshev, V. V. Kazalov, V. V. Kuzminov, S. I. Panasenko, and S. S. Ratkevich, Phys. Rev. C **87**, 035501 (2013).

[31] J. Suhonen, Phys. Rev. C **86**, 024301 (2012).

[32] M. Doi and T. Kotani, Prog. Theor. Phys. **87**, 1207 (1992).

[33] A. Gando, Y. Gando, T. Hachiya, A. Hayashi, S. Hayashida, H. Ikeda, K. Inoue, K. Ishidoshiro, Y. Karino, M. Koga, S. Matsuda, T. Mitsui, K. Nakamura, S. Obara, T. Oura, H. Ozaki, I. Shimizu, Y. Shirahata, J. Shirai, A. Suzuki *et al.* (KamLAND-Zen Collaboration), Phys. Rev. Lett. **117**, 082503 (2016).

[34] F. T. Avignone, S. R. Elliott, and J. Engel, Rev. Mod. Phys. **80**, 481 (2008).

[35] H. T. Li and Z. Z. Ren, Phys. Rev. C **96**, 065503 (2017).

[36] M. Honma, T. Otsuka, B. A. Brown, and T. Mizusaki, Phys. Rev. C **69**, 034335 (2004).

[37] M. Honma, T. Otsuka, B. Brown, and T. Mizusaki, Eur. Phys. J. A **25**, 499 (2005).

[38] A. Poves, J. Sanchez-Solano, E. Caurier, and F. Nowacki, Nucl. Phys. A **694**, 157 (2001).

[39] W. A. Richter, M. G. van der Merwe, R. E. Julies, and B. A. Brown, Nucl. Phys. A **523**, 325 (1991).

[40] J. Chen, B. Singh, and J. A. Cameron, Nucl. Data Sheets **112**, 2357 (2011); S.-C. Wu, *ibid.* **91**, 1 (2000); T. W. Burrows, *ibid.* **107**, 1747 (2006); Z. Elekes, J. Timar, and B. Singh, *ibid.* **112**, 1 (2011); J. Huo and D. Yang, *ibid.* **128**, 185 (2015); **121**, 1 (2014); C. D. Nesaraja, S. D. Geraedts, and B. Singh, *ibid.* **111**, 897 (2010); E. Browne and J. K. Tuli, *ibid.* **111**, 1093 (2010); E. A. McCutchan, *ibid.* **113**, 1735 (2012); G. Gürdal and E. A. McCutchan, *ibid.* **136**, 1 (2016).

[41] G. Martínez-Pinedo, A. Poves, E. Caurier, and A. P. Zuker, Phys. Rev. C **53**, R2602(R) (1996).

[42] M. Bernas, Ph. Dessagne, M. Langevin, J. Payet, F. Pougheon, and P. Roussel, Phys. Lett. B **113**, 279 (1982).

[43] O. Sorlin, S. Leenhardt, C. Donzaud, J. Duprat, F. Azaiez, F. Nowacki, H. Grawe, Z. Dombrádi, F. Amorini, A. Astier, D. Baiborodin, M. Belleguic, C. Borcea, C. Bourgeois, D. M. Cullen, Z. Dlouhy, E. Dragulescu, M. Górska, S. Grévy, D. Guillemaud-Mueller *et al.*, Phys. Rev. Lett. **88**, 092501 (2002).
[44] N. Mărginean *et al.*, Phys. Rev. Lett. **125**, 102502 (2020).
[45] Y. Tsunoda, T. Otsuka, N. Shimizu, M. Honma, and Y. Utsuno, Phys. Rev. C **89**, 031301(R) (2014).
[46] M. Honma, T. Otsuka, T. Mizusaki, and M. Hjorth-Jensen, Phys. Rev. C **80**, 064323 (2009).
[47] D. Mücher, G. Gürdal, K.-H. Speidel, G. J. Kumbartzki, N. Benczer-Koller, S. J. Q. Robinson, Y. Y. Sharon, L. Zamick, A. F. Lisetskiy, R. J. Casperson, A. Heinz, B. Krieger, J. Leske, P. Maier-Komor, V. Werner, E. Williams, and R. Winkler, Phys. Rev. C **79**, 054310 (2009).